Source details

Journal of Composites Science

Open Access

Years currently covered by Scopus: from 2017 to 2024

Publisher: Multidisciplinary Digital Publishing Institute (MDPI)

E-ISSN: 2504-477X

Subject area: Engineering: Engineering (miscellaneous) | Materials Science: Ceramics and Composites

Source type: Journal

CiteScore 2023
5.0

SJR 2023
0.583

SNIP 2023
1.012

View all documents > | Set document alert | Save to source list

CiteScore | CiteScore rank & trend | Scopus content coverage

CiteScore 2023

$$5.0 = \frac{7{,}047 \text{ Citations } 2020 - 2023}{1{,}419 \text{ Documents } 2020 - 2023}$$

Calculated on 05 May, 2024

CiteScoreTracker 2024

$$5.2 = \frac{8{,}024 \text{ Citations to date}}{1{,}558 \text{ Documents to date}}$$

Last updated on 05 September, 2024 • Updated monthly

CiteScore rank 2023

Category	Rank	Percentile
Engineering Engineering (miscellaneous)	#48/204	76th
Materials Science Ceramics and Composites	#47/127	63rd

View CiteScore methodology > | CiteScore FAQ > | Add CiteScore to your site

About Scopus

What is Scopus

Content coverage

Scopus blog

Scopus API

Privacy matters

Language

日本語版を表示する

查看简体中文版本

查看繁體中文版本

Просмотр версии на русском языке

Customer Service

Help

Tutorials

Contact us

Journal of Composites Science

COUNTRY

Switzerland

Universities and research institutions in Switzerland

Media Ranking in Switzerland

SUBJECT AREA AND CATEGORY

Engineering
Engineering (miscellaneous)

Materials Science
Ceramics and Composites

PUBLISHER

Multidisciplinary Digital Publishing Institute (MDPI)

H-INDEX

38

PUBLICATION TYPE

Journals

ISSN

2504477X

COVERAGE

2017-2023

INFORMATION

Homepage

How to publish in this journal

jcs@mdpi.com

SCOPE

The journal scope includes the following areas, although research in related fields may also be considered. Fiber reinforced composites; Novel composites; Nanocomposites; Biomedical composites; Energy composites; Modeling, non-destructive evaluation; Processing and manufacturing, properties and performance; Repair, testing, nano technology; Physics, chemistry and mechanics characterization of composites

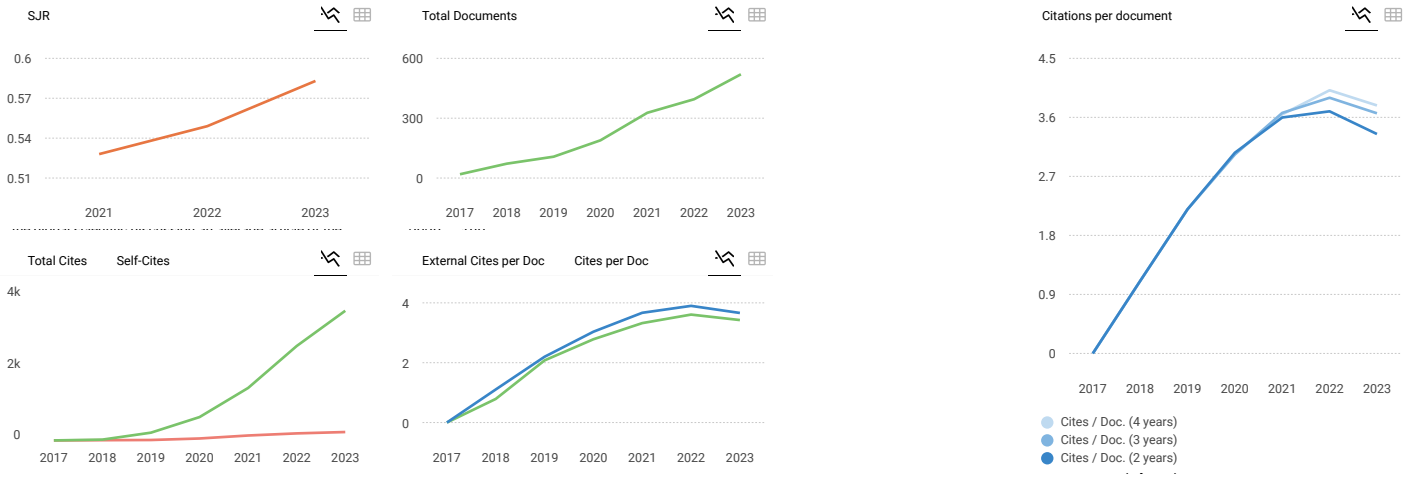

← Show this widget in your own website

Just copy the code below and paste within your html code:

<a href="https://www.scim

SCImago Graphica

Explore, visually communicate and make sense of data with our **new data visualization tool**.

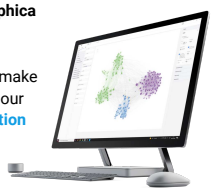

Metrics based on Scopus® data as of March 2024

S **Sengphet** 2 years ago

I am interested in this Journal

reply

Leave a comment

Name

Email
(will not be published)

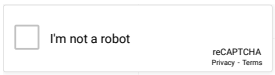

Submit

The users of Scimago Journal & Country Rank have the possibility to dialogue through comments linked to a specific journal. The purpose is to have a forum in which general doubts about the processes of publication in the journal, experiences and other issues derived from the publication of papers are resolved. For topics on particular articles, maintain the dialogue through the usual channels with your editor.

Journal of
Composites Science

IMPACT FACTOR 3.0

CITESCORE 5.0

Article

Nitrogen-Doped Borophene Quantum Dots: A Novel Sensing Material for the Detection of Hazardous Environmental Gases

Kriengkri Timsorn and Chatchawal Wongchoosuk

Special Issue
Theoretical and Computational Investigation on Composite Materials

Edited by
Prof. Dr. Zhong Hu

MDPI

https://doi.org/10.3390/jcs8100397

Journal of
Composites Science

MDPI

Article

Nitrogen-Doped Borophene Quantum Dots: A Novel Sensing Material for the Detection of Hazardous Environmental Gases

Kriengkri Timsorn [1] and Chatchawal Wongchoosuk [2,*]

[1] Division of Physics, Faculty of Science and Technology, Phetchabun Rajabhat University, Phetchabun 67000, Thailand; timsorn23@pcru.ac.th
[2] Department of Physics, Faculty of Science, Kasetsart University, Chatuchak, Bangkok 10900, Thailand
* Correspondence: chatchawal.w@ku.ac.th; Tel.: +66-2-562-5555

Abstract: Toxic gases emitted by industries and vehicles cause environmental pollution and pose significant health risks which are becoming increasingly dangerous. Therefore, the detection of the toxic gases is crucial. The development of gas sensors with high sensitivity and fast response based on nanomaterials has garnered significant interest. In this work, we studied the adsorption behavior of B_9^- wheel structures of pristine and nitrogen functionalized borophene quantum dots for major hazardous environmental gases, such as NO_2, CO_2, CO, and NH_3. The self-consistent-charge density-functional tight-binding method (SCC-DFTB) method was performed to investigate structural geometries, the most favorable adsorption sites, charge transfer, total densities of states, and electronic properties of the structures before and after adsorption of the gas molecules. Based on calculated results, it was found that the interaction between the borophene quantum dots and the gas molecules was chemisorption. The functionalized nitrogen atom contributed to impurity states, leading to higher adsorption energies of the functionalized borophene quantum dots compared to the pristine ones. Total densities of states revealed insights into electronic properties of gas molecules adsorbed on borophene quantum dots. The nitrogen-doped borophene quantum dots demonstrated excellent performance as a sensing material for hazardous environmental gases, especially CO_2.

Keywords: borophene quantum dot; SCC-DFTB; toxic gas; gas adsorption; gas sensor

Citation: Timsorn, K.; Wongchoosuk, C. Nitrogen-Doped Borophene Quantum Dots: A Novel Sensing Material for the Detection of Hazardous Environmental Gases. *J. Compos. Sci.* **2024**, *8*, 397. https://doi.org/10.3390/jcs8100397

Academic Editor: Zhong Hu

Received: 2 August 2024
Revised: 18 September 2024
Accepted: 26 September 2024
Published: 1 October 2024

1. Introduction

Hazardous gases (such as CO_x, NO_x, and NH_3) produced by industrial activities and vehicles cause respiratory diseases in humans, contribute to the greenhouse effect, and damage the environment [1]. For the safety of human health and environmental protection, gas sensor technology is crucial for the detection of these gases. Due to unique properties of nanomaterials, two-dimensional materials such as graphene, silicene, Mxene, phosphorene, and transition metal dichalcogenides have attracted significant interest in various studies [2–8]. For gas sensing applications, graphene exhibits great performance due to its excellent mobility and high surface-to-volume ratio [9–11]. However, the absence of a band gap in graphene makes it difficult to control charge in the sheet [9,12]. Borophene, a two-dimensional material composed of monolayer of boron atoms, has been successfully synthesized on silver surface under ultrahigh vacuum conditions [13,14]. Borophene has gained widespread attraction for research in nanotechnology because of its unique electronic, optical, thermal, magnetic, and mechanical properties [15–19]. Boron possesses three valence electrons in $2s^2 2p^1$ orbitals which can form sp^2 hybridization [9,15] and the bonding between boron atoms is highly complex with polymorphisms [13]. This complexity leads to various physical and chemical properties [20,21], which distinguish it from other two-dimensional materials like graphene and transition metal dichalcogenides. Owing to a variety of atomic arrangements, there have been reports on theoretical and experimental studies of borophene structures with several stable structures including triangular and hexagonal planar or quasi-planar structure motifs [17,22–26]. An anionic B_9 cluster (B_9^-) is

a highly symmetric planar wheel-like structure of borophene composed of a single boron atom at the center of a B_8 ring [27,28]. The structure provides double aromaticity and high electronic stability resulting from the bonding between the central boron atom and the B_8 ring through three delocalized σ and three delocalized π bonds [27]. Doping with metal atoms can modify the structures and properties of borophene with small planar or quasi-planar structures tailored for specific applications [27,29–32]. The structural diversity offers enormous potential to tailor the properties of borophene for applications in areas ranging from electronics [33,34], energy storage [35,36], gas sensing [9,37,38], etc.

Focusing on gas sensing applications, the extraordinary geometries, high surface-to-volume ratio, and excellent electronic properties of borophene allow it to be used as gas sensors. Several theoretical studies have reported on the adsorption of gas molecules by borophene. For examples, Huang et al. [37] calculated adsorption energies, charge transfer, and electronic structures of borophene with buckled and line-defective phases for adsorption of NH_3, NO, NO_2, and CO using density functional theory (DFT). Shukla et al. [9] used DFT calculation combined with non-equilibrium Green's function (NEGF) to study adsorption behavior of monolayer borophene for gas molecules of CO, CO_2, NO, NO_2, and NH_3. Ta et al. [38] theoretically investigated the potential for the adsorption of five main hazardous gases including CO, NO, NH_3, NO_2, and CO_2 on β_{12} borophene by using van der Waals (vdW) density functionals (vdW-DFs). These studies showed that borophene could be developed as sensing materials for gas sensors to detect toxic gases. However, the mentioned studies focused on gas adsorption of pristine borophene sheets with different structures.

Recently, borophene quantum dots (BQDs) have been explored for various applications, including solar cell [39], biosensors [40,41], catalysts [42], supercapacitors [43], and biomedical applications [44]. For instance, Liu et al. reported the preparation of BQDs/BC_2N heterostructures for an ultrasensitive humidity sensor. The sensor showed ultra-high sensitivity, high selectivity, fast response and recovery times, and good flexibility over a wide detection range (11–97% RH) by using the Grotthuss chain reaction sensing mechanism via hydrogen bonding and multilayer physisorption [45]. The BQDs exhibit quantum confinement effects, where their electronic and optical properties are influenced by the size and shape of the dots [40,46]. However, research on the application of pristine and chemically functionalized BQDs for gas sensing application is still limited.

In the present study, we theoretically investigate the adsorption behaviors of NO_2, CO_2, CO, and NH_3 gas molecules on B_9^- wheel structures of pristine and nitrogen functionalized BQDs using self-consistent charge density functional tight-binding (SCC-DFTB) method. We examine adsorption energies, optimal adsorption sites, charge transfer, density of states (DOS), and electronic properties to understand the interaction between these gas molecules and the pristine and nitrogen functionalized BQDs.

2. Calculation Methods

The SCC-DFTB method is derived from second-order expansion of the DFT Kohn–Sham total energy in terms of the charge density fluctuations [47–49]. The Kohn–Sham approach simplifies the complex problem of interacting electrons by mapping it onto a system of non-interacting electrons that reproduce the same electron density. Although the non-interacting system is easier to solve, it still provides the correct ground-state electron density for the original interacting system. In the DFTB approach, the traditional self-consistency between the effective potential and the charge density is replaced by a simpler self-consistency in the distribution of Mulliken charges. The method is optimized for high accuracy by using a minimal basis set to represent the single-electron Kohn–Sham-like eigenstates. This allows electronic interactions to be precomputed within a two-center model using an effective Hamiltonian derived from a carefully chosen reference density [50].

Based on Kohn–Sham orbitals, the total energy for the SCC-DFTB method is expressed as [51,52]:

$$E_{tot}^{SCC\text{-}DFTB} = \sum_{i} \langle \phi_i | \hat{H}_0 | \phi_i \rangle + \frac{1}{2} \sum_{A,B} \gamma_{AB} \Delta q_A \Delta q_B + E_{rep} \quad (1)$$

where ϕ_i is the Kohn–Sham orbitals, $\hat{H}_0$ is unperturbed Hamiltonian, Δq_A and Δq_B are the induced charges on the atoms A and B, respectively, γ_{AB} is the second derivative with respect to its total charges (Coulombic-like interaction potential), and E_{rep} denotes repulsive potential for the pair of atoms A and B.

The benchmark of the SCC-DFTB method is a balance between accuracy and computational efficiency with reduced computational costs compared to standard DFT [47,49]. For large systems, the SCC-DFTB calculations were 2–3 orders of magnitude faster than DFT [47,51]. It should be noted that that calculation time depends on both the number of atoms and the complexity of the structures being simulated. While the system in this work may not be considered large in absolute terms, SCC-DFTB still ensures faster computation times. The SCC-DFTB method simulates electronic properties, energies, and molecular structures of molecules and materials, and provides results in good agreement with DFT methods [53]. For gas adsorption, the SCC-DFTB method can be used to investigate interaction between gas molecules and sensing materials [54–56]. The benchmark of the SCC-DFTB method has been performed for theoretical studies of boron clusters [52,57].

In this work, B_9^- wheel-like structures of pristine and nitrogen functionalized BQDs (B_9^- and N/B_9^- BQDs) were built. For nitrogen functionalization, a nitrogen atom was at the center of the B_9^- ring and bonded with nine surrounding boron atoms. It should be noted that this configuration is theoretically feasible because nitrogen can bond to boron forming a stable structure. However, experimental implementation can be challenging due to the precision required to control the doping process and ensure that the nitrogen atom is properly positioned at the center of the B9 ring. Techniques like molecular beam epitaxy or chemical vapor deposition which allow for atomic-level precision may be required making the process more complex but achievable with advanced fabrication methods. To reduce the impact of edge effects, we applied periodic boundary conditions along with a large simulation box to investigate the QDs. This approach ensures that the QDs' electronic structure, adsorption phenomena, and charge transfer effects are accurately accounted for providing more reliable insights compared to calculations using a single unit cell. The matsci-0-3 parameter set was used for calculation in O-N-C-B-H system. In addition, the matsci-0-3 parameter set well describes the interaction of covalent organic system, especially small organic molecules containing nitrogen, oxygen, carbon, and hydrogen [49,51,58,59]. The SCC-DFTB command code and its relative parameters are demonstrated in Source Code S1 of Supporting Information. To investigate the most favorable adsorption sites, gas molecules including NO_2, CO_2, CO, and NH_3 were placed at different distances with orientation configurations (parallel and perpendicular) above the surfaces of B_9^- and N/B_9^- BQDs. Adsorption strengths between the structures and gas molecules are described in the term of adsorption energies (E_{ad}). The adsorption energy is calculated as the following equation:

$$E_{ad} = E_{tot}(\text{BQDs} + \text{gas molecules}) - E_{tot}(\text{BQDs}) - E_{tot}(\text{gas molecules}) \quad (2)$$

where $E_{tot}(\text{BQDs} + \text{gas molecules})$, $E_{tot}(\text{BQDs})$, and $E_{tot}(\text{gas molecules})$ are the total energies of B_9^- or N/B_9^- BQDs with gas molecules, BQDs, and gas molecules, respectively. A negative value of E_{ad} indicates that gas molecules are adsorbed and more negative values are more favorable adsorption sites.

To study charge transfers from/to gas molecules resulting from the adsorption, net charge transfer is defined as the charge difference of gas molecules before and after adsorption [60]. The net charge transfer (Q) is obtained from Equation (3):

$$Q = Q(\text{BQDs} + \text{gas molecules}) - Q(\text{gas molecules}) \quad (3)$$

where Q(BQDs + gas molecules) and Q(gas molecules) are the charges of gas molecules adsorbed on the surfaces of BQDs structures and isolated gas molecules, respectively.

Total density of states (DOS) was calculated to analyze the influence of gas molecule adsorption on the electronic properties of BQDs. The k-point sampling density was set to 5 × 5 × 1 for the DOS studies [37].

3. Results and Discussion

3.1. Structural and Electronic Properties of B_9^- and N/B_9^- BQDs

Figure 1a shows the optimized structures of B_9^- and N/B_9^- BQDs with side and top views. These structures were optimized to obtain the most stable structure. During the optimization process, the initial geometries of the BQD structures were input into the SCC-DFTB framework. The energy minimization was performed iteratively by adjusting atomic positions with the forces on each atom being calculated at each step. The optimization continued until the system reached a stable configuration where the forces on the atoms were below a predefined threshold and the total energy converged. An example of SCC-DFTB optimization command code is provided in Source Code S1 of the Supporting Information.

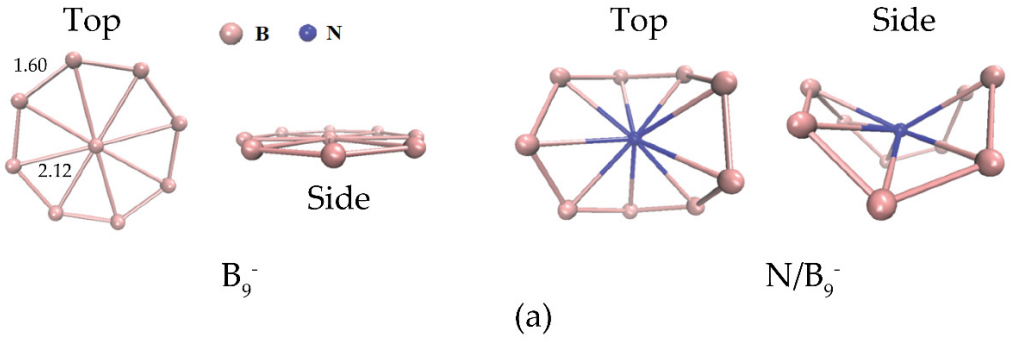

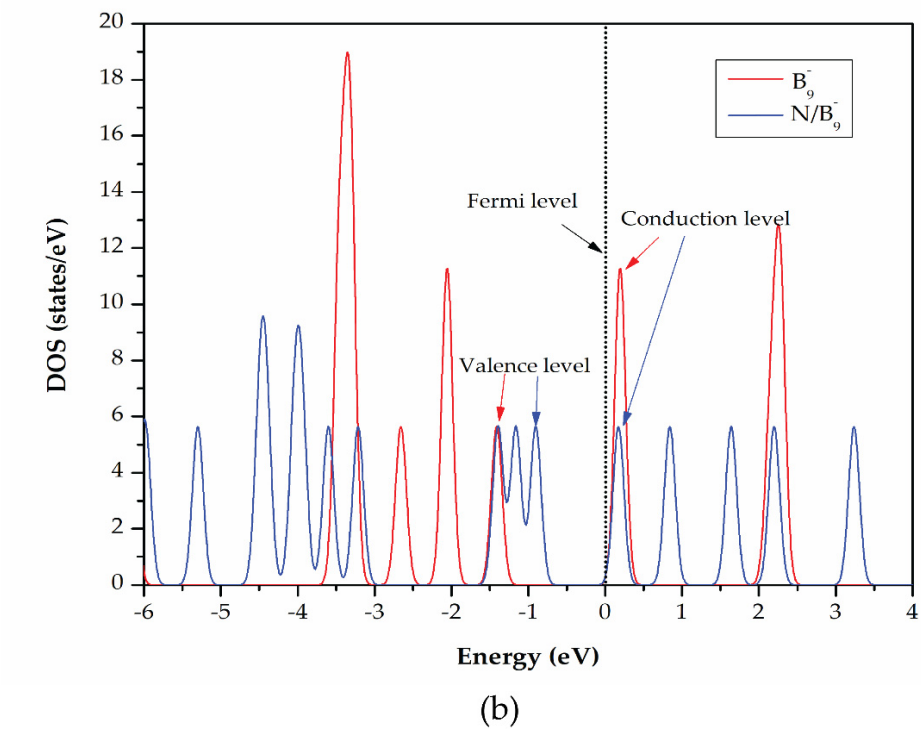

Figure 1. (**a**) Side and top views of the optimized structures of B_9^- and N/B_9^- BQDs and (**b**) DOS of the structures.

For the B_9^- BQDs, it was found that the bond lengths between the central boron atom and each boron atom of the B_8 ring are ~2.12 Å. The structural diameter and the bond lengths between boron atoms on the B_8 ring side are ~4.22 Å and ~1.60 Å, respectively. The bond lengths of our optimized B_9^- BQD structures show good agreement with previously published studies [27,32]. In addition, the structures of all planar boron clusters have been experimentally confirmed to consist of an outer boron atom ring and one or more inner atoms [27]. The central boron atom contributes all three valence electrons to the delocalized bonding [27]. The boron atoms in the ring side contribute their two valence electrons to two-center, two-electron (2c–2e) boron–boron bonds of the ring, while the remaining valence electron participates in delocalized σ and π bonding with the central boron atom [27,61,62]. For nitrogen functionalization, a nitrogen atom (blue color) was placed at the center of the ring. It can be obviously seen that the structural distortion occurred which corresponds to the previous work [63]. The structure is buckled where some boron atoms move inward or outward with respect to the central nitrogen atom. The distortion arises from the inherent nature of borophene with boron atoms forming triangles or hexagons in which nitrogen doping can induce structural distortions. The bond lengths between the boron atoms on the ring side and the central nitrogen atom are changed to be in the range of 1.88–2.00 Å.

To study electronic properties of B_9^- and N/B_9^- BQDs, we calculated energy gap (E_g), E_{LUMO}, E_{HOMO}, Fermi energy (E_F), and DOS as presented in Table 1 and Figure 1b. It was found that E_g decreases significantly from 2.72 eV to 0.68 eV after nitrogen functionalization. The large decrease of E_g results from a change in energy levels of the conduction band edge (E_{LUMO}) and the valence band edge (E_{HOMO}), as shown in Table 1. The conduction band edge shifts downward and the valence band edge shifts upward. This result reveals that nitrogen functionalization at the center of the boron ring introduces impurity states within the band structure of B_9^- BQDs. The interaction between these impurity states and an additional electron, which occupy in the conduction band or near the conduction band edge in the B_9^- structure, modifies the energy levels near the Fermi level resulting in the reduced energy gap [64,65]. Figure 1b shows the calculated DOS of B_9^- and N/B_9^- BQDs. It should be noted that the DOS describes the distribution of electronic states as a function of energy. It can be clearly seen that new DOS peaks (blue lines) around the vicinity of the Fermi level appeared after nitrogen functionalization. This confirms that nitrogen functionalization creates new localized states due to the difference in electronic configuration of nitrogen atoms compared to boron atoms [66], which indicates the presence of electrons or holes. The E_g values from Table 1 correspond well with those shown in Figure 1b.

Table 1. Electronic parameter of B_9^- and N/B_9^- BQDs.

Structure	E_{HOMO} (eV)	E_{LUMO} (eV)	E_F (eV)	E_g (eV)
B_9^-	−6.18	−3.46	−6.15	2.72
N/B_9^-	−5.98	−5.30	−5.64	0.68

3.2. Adsorption of NO_2, CO_2, CO, and NH_3 Gas Molecules on B_9^- BQDs

To investigate the adsorption behavior of B_9^- BQDs for the detection of NO_2, CO_2, CO, and NH_3 gas molecules, the different adsorption structures were constructed and fully optimized. Each gas molecule was placed on the top of the B_9^- BQD structures with both parallel and perpendicular orientations. Each atom of these gas molecules was pointed toward a boron atom of the structures including N-B, C-B, O-B, and H-B to find the most favorable adsorption sites. Figure 2 shows side and top views of some optimized B_9^- BQD structures with gas molecules on the top of the structures in parallel and perpendicular orientations. The typical calculated adsorption parameters are summarized in Table 2. Based on overview of the calculated E_{ad} values, it is found that the highest to lowest E_{ad} values are found for NO_2, CO, CO_2, and NH_3, respectively. In each case, the E_{ad} values are higher than adsorption energies of borophene sheets for these toxic gases [9,37]. This result

reveals that quantum confinement effects and high surface to volume ratio of the BQDs improve the adsorption performance for gas sensing. For charge transfer calculation, the most values of charge transfer are found to be positive which is consistent with published work [38]. Also, large charge transfer is found for all gas molecules. The positive (negative) sign of charge transfer shows that gas molecules accept (donate) electrons [38].

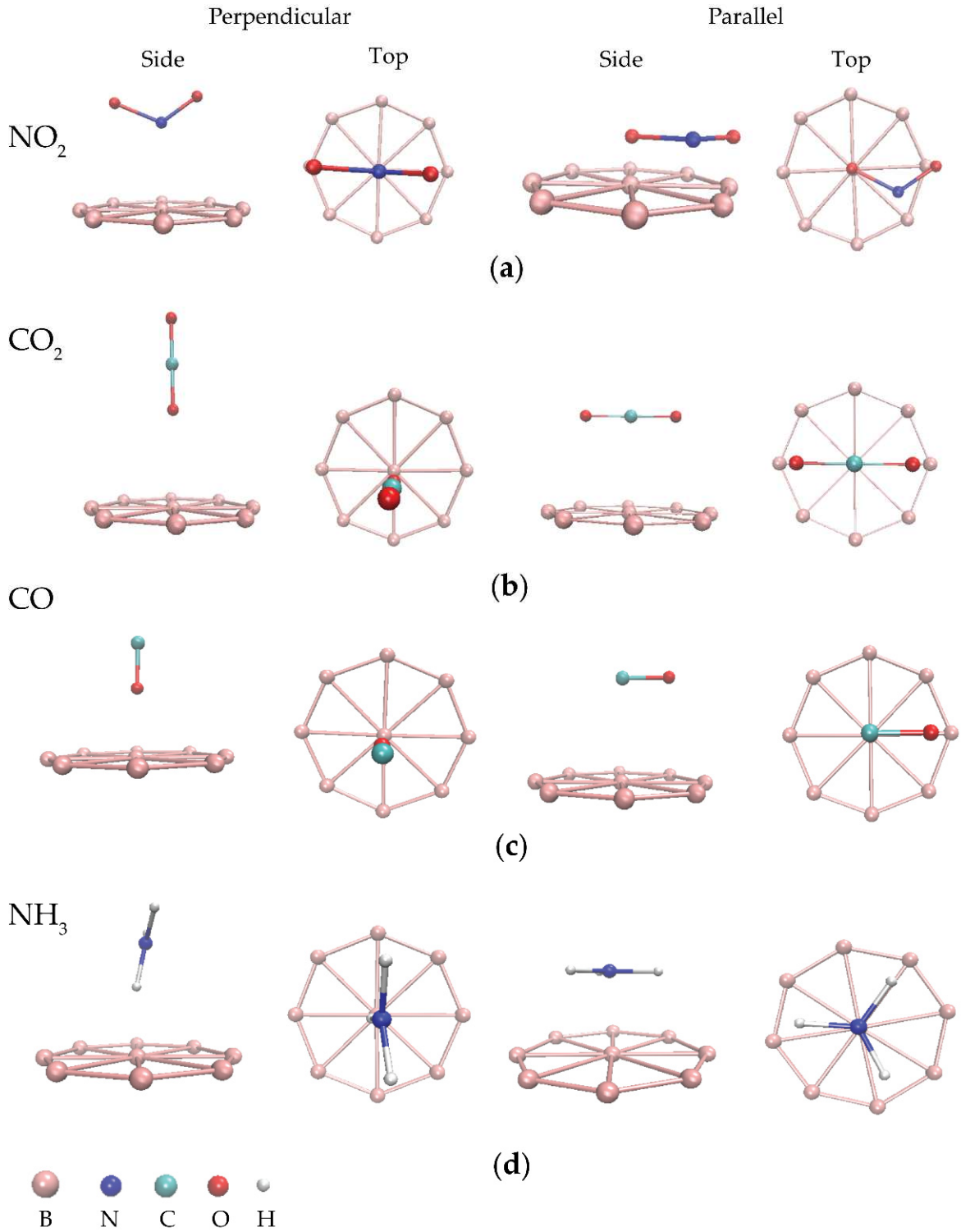

Figure 2. Side and top views of some optimized B_9^- BQDs for adsorption of (**a**) NO_2, (**b**) CO_2, (**c**) CO, and (**d**) NH_3 with perpendicular and parallel orientations.

Table 2. Typical calculated adsorption parameters for each gas molecule absorbed on the B_9^- BQD structures.

System	Orientation	Adsorption Site	Distance (Å)	E_{ad} (eV)	Q (e)	E_{HOMO} (eV)	E_{LUMO} (eV)	E_g (eV)
$B9^-$-NO_2	parallel	B-N	1.23	−5.80	0.273	−5.81	−4.31	1.50
		B-O	2.25	−4.39	0.218	−5.94	−4.99	0.95
	perpendicular	B-N	2.97	−4.39	0.218	−5.94	−4.99	0.95
		B-O	3.00	−6.52	0.166	−5.59	−4.56	1.03
B_9^--CO	parallel	B-C	1.01	−8.47	−0.164	−5.42	−4.41	1.01
		B-O	1.12	−6.82	−0.317	−6.12	−5.30	0.82
	perpendicular	B-C	2.41	−2.04	0.370	−5.61	−3.44	2.17
		B-O	1.04	−0.72	0.341	−5.65	−3.39	2.26
B_9^--CO_2	parallel	B-C	1.75	−6.66	0.131	−5.26	−4.49	0.77
		B-O	1.72	−3.93	−0.027	−5.83	−4.61	1.22
	perpendicular	B-C	2.20	−0.61	0.470	−5.07	−2.63	2.44
		B-O	1.34	−0.60	0.467	−5.09	−2.88	2.21
B_9^--NH_3	parallel	B-N	3.00	−1.77	0.421	−5.16	−2.77	2.39
		B-H	3.58	−1.78	0.420	−5.14	−2.90	2.24
	perpendicular	B-N	1.00	−4.06	0.083	−5.22	−4.21	1.01
		B-H	2.50	−1.78	0.420	−5.14	−2.90	2.24

To consider the adsorption sites of each gas molecule, the most favorable adsorption sites for NO_2, CO, CO_2, and NH_3 were identified as B-O (perpendicular), B-C (parallel), B-C (parallel), and B-N (perpendicular), respectively. Interestingly, both CO and CO_2 prefer B-C adsorption sites with parallel orientation. In case of energy gap, it can be obviously seen that the energy gap decreases for all adsorption sites of all gas molecules, which suggests that conductivity of the B_9^- BQDs increases after gas adsorption. Based on the results of Table 2, high adsorption energies, large charge transfer, and short interaction distances reveal that the interaction between gas molecules and the B_9^- BQDs is a result of chemisorption [9,37,38]. Additionally, further adsorption sites on the BQDs were investigated, as presented in Figure S1 and Table S1 of the Supporting Information. However, the results from these additional sites were less favorable due to weaker adsorption energies and interactions, resulting in less stable configurations. Therefore, only the perpendicular and parallel orientations were selected for this study.

3.3. Adsorption of NO_2, CO_2, CO, and NH_3 Gas Molecules on N/B_9^- BQDs

Figure 3 displays some optimized N/B_9^- BQD structures for adsorption of NO_2, CO_2, CO, and NH_3 gas molecules at different interaction distances. The calculated adsorption parameters are presented in Table 3. Each atom of gas molecules was placed on the top of the N/B_9^- BQD structures pointing to the nitrogen atom with parallel and perpendicular orientation. According to the results of Table 3, the results shows that the E_{ad} values of the N/B_9^- BQDs for all gas molecules at all adsorption sites obviously increased in comparison with the E_{ad} values of the B_9^- BQDs. The favorable adsorption sites for NO_2, CO, and CO_2 are parallel orientation, except for NH_3, which preferred perpendicular orientation. The highest E_{ad} values of CO_2, CO, NO_2, and NH_3 at their most favorable adsorption sites are −16.57, −12.08, −11.64, and −7.22 eV, respectively. There are two reasons that can describe this result. First, the functionalized nitrogen atom introduces impurity states leading to strong interaction. Second, the buckling of the N/B_9^- BQDs allows gas atoms bonding with more than one surrounding boron atoms [37]. Looking at charge transfer, it is found that the most charge transfer is positive and lower than that of the $B9^-$ BQDs. This demonstrates that the trend in charge transfer of each gas molecule is still from the structures to gas molecules. It is attributed that the lower charge transfer results from strong interaction (high E_{ad} values), localized electronic states from impurities and buckled surface of the N/B_9^- BQDs, which affects pathway of charge transfer. The

interaction distances for all adsorption sites are in the range of chemical bonding indicating chemisorption [38].

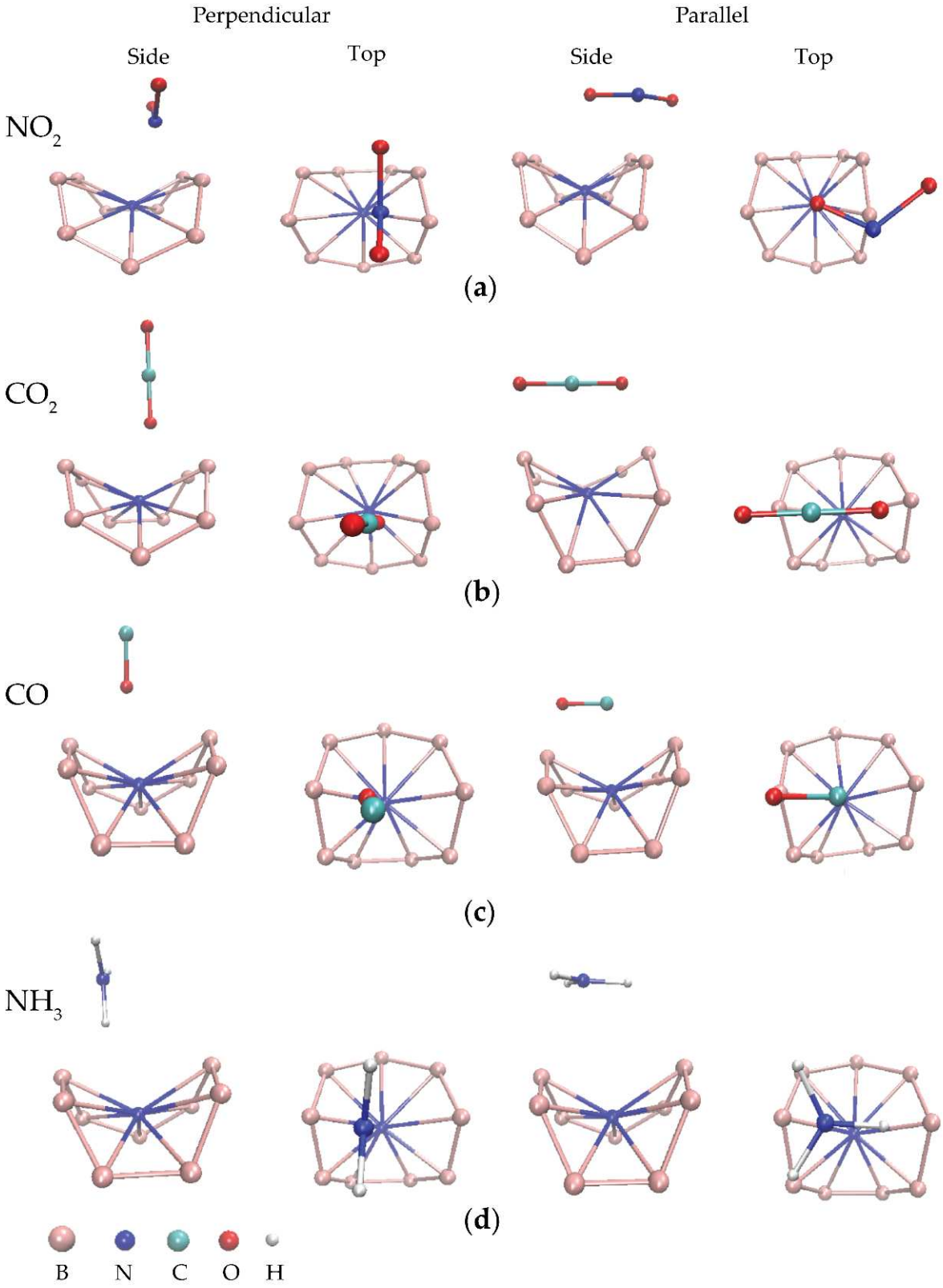

Figure 3. Side and top views of some optimized N/B_9^- BQDs for adsorption of (**a**) NO_2, (**b**) CO_2, (**c**) CO, and (**d**) NH_3 with perpendicular and parallel orientations.

Table 3. Typical calculated adsorption parameters for each gas molecule absorbed on the N/B_9^- BQD structures.

System	Orientation	Adsorption Site	Distance (Å)	E_{ad} (eV)	Q (e)	E_{HOMO} (eV)	E_{LUMO} (eV)	E_g (eV)
N/B_9^--NO_2	parallel	N-N	1.00	−11.64	0.021	−5.04	−4.55	0.49
		N-O	2.52	−8.67	0.036	−5.24	−4.29	0.95
	perpendicular	N-N	1.15	−6.99	0.014	−5.35	−4.52	0.83
		N-O	3.10	−8.67	0.036	−5.24	−4.29	0.95
N/B_9^--CO	parallel	N-C	1.15	−12.08	0.105	−5.17	−4.56	0.61
		N-O	1.34	−7.86	−0.117	−5.42	−4.82	0.60
	perpendicular	N-C	1.65	−4.28	0.166	−6.03	−5.71	0.32
		N-O	1.80	−4.60	0.147	−5.62	−4.79	0.83
N/B_9^--CO_2	parallel	N-C	1.25	−16.57	−0.086	−5.92	−3.88	2.04
		N-O	1.20	−16.11	−0.466	−5.80	−4.58	1.22
	perpendicular	N-C	2.51	−6.57	0.201	−4.98	−4.18	0.80
		N-O	1.00	−3.23	0.115	−5.80	−4.90	0.90
N/B_9^--NH_3	parallel	N-H	1.02	−6.34	0.121	−5.92	−4.81	1.11
		N-N	1.14	−6.70	0.039	−5.90	−5.00	0.90
	perpendicular	N-H	1.57	−7.22	0.116	−5.41	−4.19	1.22
		N-N	1.05	−6.80	−0.049	−5.90	−4.86	1.04

For energy gap, the trend in slightly increases energy gap of the N/B_9^- BQDs after adsorption of NO_2, CO_2, and NH_3, whereas the energy gap of CO adsorbs on the structure tend to be decreased. We will explain this result in the section of DOS (in the Section 3.4). A comparison of adsorption energies with other two-dimensional materials such as graphene, for instance, exhibited weak adsorption energies for NO_2, CO_2, CO, and NH_3 gas molecules [9]. The adsorption energies of NO_2, CO and NH_3 gas molecules on borophene sheets were found to be −1.75, −1.24, and −1.45 eV, respectively [37]. In case of MoS_2, the adsorption energies were −0.44 and −0.33 eV for CO and CO_2, respectively [9]. Based on the results, nitrogen functionalization at the center of the $B9^-$ BQD ring could improve the adsorption behavior of $B9^-$ BQDs for NO_2, CO_2, CO, and NH_3 gas molecules.

3.4. Total Densities of State (DOS)

DOS calculations were performed to gain insights into the interactions between gas molecules and both B_9^- and N/B_9^- BQDs structures. Figure 4 demonstrates the calculated DOS of the most favorable adsorption sites for each gas molecule. It was observed that sharp DOS peaks appeared near the Fermi level for all gas molecules adsorbed on the N/B_9^- BQDs indicating strong bonding [38], which corresponds to higher adsorption energies than the B_9^- BQDs with gas molecules. In both cases, DOS peaks near the Fermi level suggest charge transfer from the BQDs to the gas molecules [9]. Among all these gases, only CO contributes states near the Fermi level, specifically at the top of valence band, which might improve the conductivity [37]. This confirms the decreasing energy gap in case of CO adsorbed on the N/B_9^- BQDs, which is the reason for Section 3.3. To consider in details of each case as shown in Figure 4a–d, new local states appeared near the conduction band edge for NO_2, CO_2, and NH_3 on N/B_9^- BQDs, while in case of CO-N/B_9^- BQD, a new local state appeared below the Fermi level at −0.4 eV. This suggests the existence of localized states from the impurities interacting with gas molecules.

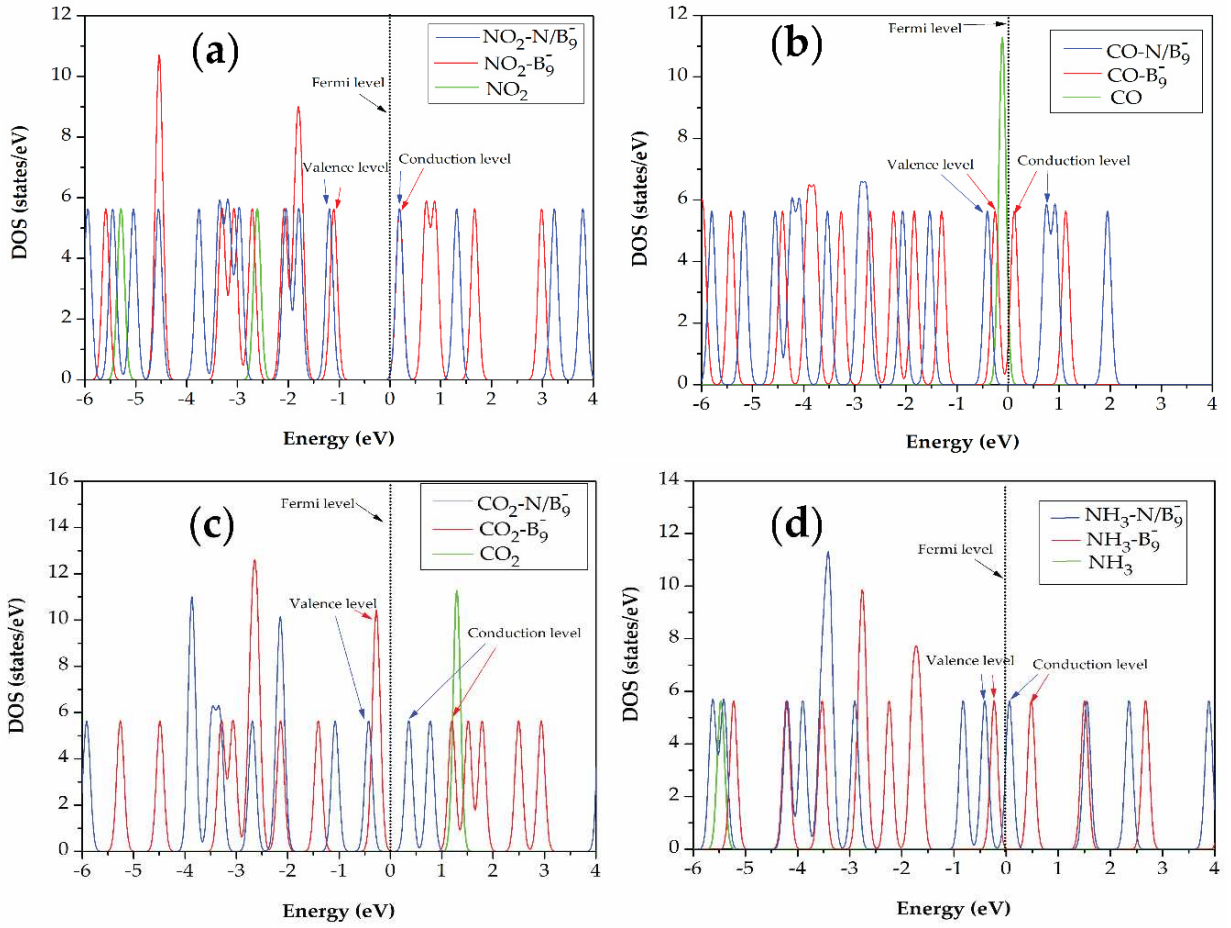

Figure 4. Calculated DOSs for (**a**) NO_2, (**b**) CO, (**c**) CO_2, and (**d**) NH_3 adsorbed on B_9^- and N/B_9^- BQDs structures. The Fermi level is set to zero with dashed vertical lines.

4. Conclusions

In summary, we have studied the adsorption behavior of B_9^- and B_9^- BQDs structures for NO_2, CO, CO_2, and NH_3 gas molecules using SCC-DFTB method. Structural geometries, the most favorable adsorption sites and electronic properties were investigated. After nitrogen functionalization, the structural and electronic properties of B_9^- BQDs were changed. The structure was buckled and its energy gap was decreased due to the impurity states. Based on the adsorption results, the adsorption energies of the structures were found to be higher than those of borophene sheets. Additionally, the adsorption energies of the B_9^- BQDs were higher than those of the B_9^- BQDs. The B_9^- BQDs favored NO_2 adsorption while the N/B9$^-$ BQDs favored CO_2 with parallel orientation. The calculated charge transfer indicated that there was a transfer of charge from the BQDs structures to the gas molecules. In case of DOS analysis, new local states formed around the Fermi level after gas adsorption. According to high adsorption energies, DOS and interaction distances, the interaction between gas molecules and the B_9^- and B_9^- BQDs was found to be chemisorption. Our calculation suggests that nitrogen-doped BQDs are promising candidates for detecting hazardous gases in the environment. We believe that this work will provide valuable guidance on future studies in both simulations and experiments.

Supplementary Materials: The following supporting information can be downloaded at: https://www.mdpi.com/article/10.3390/jcs8100397/s1, Table S1: Typical calculated adsorption parameters for each gas molecule absorbed on the BQD structures with bridge and hollow sites; Figure S1: Some optimized BQDs for adsorption of (a) NO_2, (b) CO_2, (c) CO and (d) NH_3 with bridge and hollow sites; Source Code S1: An example of DFTB command code for full optimization.

Author Contributions: Conceptualization, K.T.; methodology, K.T.; simulation, K.T.; formal analysis, K.T. and C.W.; investigation, K.T. and C.W.; data curation, K.T.; writing—original draft preparation, K.T.; writing—review and editing, C.W.; validation, C.W.; visualization, K.T.; supervision, C.W.; funding acquisition, K.T. and C.W. All authors have read and agreed to the published version of the manuscript.

Funding: This research was funded by the Thailand Science Research and Innovation (TSRI), RDI PCRU, grant number TSRI 2567/45. C.W. would like to thank the Kasetsart University Research and Development Institute (KURDI) for funding, under the grant number FF(KU)51.67.

Data Availability Statement: The original data presented in the study are included in the article; further inquiries can be directed to the corresponding author.

Acknowledgments: The authors acknowledge Laboratory for Multiscale Innovative Technologies (LMIT), Faculty of Science, Kasetsart University for computer servers.

Conflicts of Interest: The authors declare no conflicts of interest.

References

1. Seesaard, T.; Kamjornkittikoon, K.; Wongchoosuk, C. A comprehensive review on advancements in sensors for air pollution applications. *Sci. Total Environ.* **2024**, *951*, 175696. [CrossRef] [PubMed]
2. Chaloeipote, G.; Wongchoosuk, C. Flexible humidity sensor based on PEDOT:PSS/Mxene nanocomposite. *Flex. Print. Electron.* **2024**, *9*, 015015. [CrossRef]
3. Seekaew, Y.; Kamlue, S.; Wongchoosuk, C. Room-temperature ammonia gas sensor based on $Ti_3C_2T_x$ MXene/Graphene Oxide/CuO/ZnO Nanocomposite. *ACS Appl. Nano Mater.* **2023**, *6*, 9008–9020. [CrossRef]
4. Aufray, B.; Kara, A.; Vizzini, S.; Oughaddou, H.; Léandri, C.; Ealet, B.; Le Lay, G. Graphene-like silicon nanoribbons on Ag(110): A possible formation of silicene. *Appl. Phys. Lett.* **2010**, *96*, 183102. [CrossRef]
5. Liu, H.; Neal, A.T.; Zhu, Z.; Luo, Z.; Xu, X.; Tománek, D.; Ye, P.D. Phosphorene: An unexplored 2D semiconductor with a high hole mobility. *ACS Nano* **2014**, *8*, 4033–4041. [CrossRef]
6. Pumera, M.; Sofer, Z.; Ambrosi, A. Layered transition metal dichalcogenides for electrochemical energy generation and storage. *J. Mater. Chem. A* **2014**, *2*, 8981–8987. [CrossRef]
7. Chen, X.; Hu, J.; Chen, P.; Yin, M.; Meng, F.; Zhang, Y. UV-light-assisted NO_2 gas sensor based on WS_2/PbS heterostructures with full recoverability and reliable anti-humidity ability. *Sens. Actuators B Chem.* **2021**, *339*, 129902. [CrossRef]
8. Pak, Y.; Lim, N.; Kumaresan, Y.; Lee, R.; Kim, K.; Kim, T.H.; Kim, S.M.; Kim, J.T.; Lee, H.; Ham, M.H.; et al. Palladium nanoribbon array for fast hydrogen gas sensing with ultrahigh sensitivity. *Adv. Mater.* **2015**, *27*, 6945–6952. [CrossRef]
9. Shukla, V.; Wärma, J.; Jena, N.K.; Grigoriev, A.; Ahuja, R. Toward the realization of 2D borophene based gas sensor. *J. Phys. Chem. C* **2017**, *121*, 26869–26876. [CrossRef]
10. Yuan, W.; Shi, G. Graphene-based gas sensors. *J. Mater. Chem. A* **2013**, *1*, 10078. [CrossRef]
11. Wang, T.; Huang, D.; Yang, Z.; Xu, S.; He, G.; Li, X.; Hu, N.; Yin, G.; He, D.; Zhang, L. A review on graphene-based gas/vapor sensors with unique properties and potential applications. *Nano-Micro Lett.* **2016**, *8*, 95–119. [CrossRef] [PubMed]
12. Castro Neto, A.H.; Guinea, F.; Peres, N.M.R.; Novoselov, K.S.; Geim, A.K. The electronic properties of graphene. *Rev. Mod. Phys.* **2009**, *81*, 109–162. [CrossRef]
13. Mannix, A.J.; Zhou, X.-F.; Kiraly, B.; Wood, J.D.; Alducin, D.; Myers, B.D.; Liu, X.; Fisher, B.L.; Santiago, U.; Guest, J.R.; et al. Synthesis of borophenes: Anisotropic, two-dimensional boron polymorps. *Science* **2015**, *350*, 1513–1516. [CrossRef] [PubMed]
14. Feng, B.; Zhang, J.; Zhong, Q.; Li, W.; Li, S.; Li, H.; Cheng, P.; Meng, S.; Chen, L.; Wu, K. Experimental realization of two-dimensional boron sheets. *Nat. Chem.* **2016**, *8*, 563–568. [CrossRef] [PubMed]
15. Kaneti, Y.V.; Benu, D.P.; Xu, X.; Yuliarto, B.; Yamauchi, Y.; Golberg, D. Borophene: Two-dimensional boron monolayer: Synthesis, properties, and potential applications. *Chem. Rev.* **2022**, *122*, 1000–1051. [CrossRef]
16. Hou, C.; Tai, G.; Liu, Y.; Liu, X. Borophene gas sensor. *Nano Res.* **2022**, *15*, 2537–2544. [CrossRef]
17. Zhang, Z.H.; Penev, E.S.; Yakobson, B.I. Two-dimensional boron: Structures, properties and applications. *Chem. Soc. Rev.* **2017**, *46*, 6746–6763. [CrossRef]
18. Sergeeva, A.P.; Popov, I.A.; Piazza, Z.A.; Li, W.L.; Romanescu, C.; Wang, L.S.; Boldyrev, A.I. Understanding boron through size-selected clusters: Structure, chemical bonding, and fluxionality. *Acc. Chem. Res.* **2014**, *47*, 1349–1358. [CrossRef]
19. Hou, C.; Tai, G.A.; Wu, Z.H.; Hao, J.Q. Borophene: Current status, challenges and opportunities. *ChemPlusChem* **2020**, *85*, 2186–2196. [CrossRef]
20. Sabokdast, S.; Horri, A.; Azar, Y.T.; Momeni, M.; Tavakoli, M.B. Detection of nucleobases on borophene nanosheet: A DFT investigation. *Bioelectrochemistry* **2021**, *138*, 107721. [CrossRef]
21. Wang, Z.-Q.; Lü, T.-Y.; Wang, H.-Q.; Feng, Y.P.; Zheng, J.-C. Review of borophene and its potential applications. *Front. Phys.* **2019**, *14*, 33403. [CrossRef]
22. Yang, X.; Ding, Y.; Ni, J. Ab initio prediction of stable boron sheets and boron nanotubes: Structure, stability, and electronic properties. *Phys. Rev. B* **2008**, *77*, 041402. [CrossRef]

23. Liu, Y.; Penev, E.S.; Yakobson, B.I. Probing the synthesis of two-dimensional boron by first-principles computations. *Angew. Chem.* **2013**, *52*, 3156–3159. [CrossRef] [PubMed]
24. Zhang, Z.; Yang, Y.; Gao, G.; Yakobson, B.I. Two-dimensional boron monolayers mediated by metal substrates. *Angew. Chem.* **2015**, *127*, 13214–13218. [CrossRef]
25. Penev, E.S.; Bhowmick, S.; Sadrzadeh, A.; Yakobson, B.I. Polymorphism of two-dimensional boron. *Nano Lett.* **2012**, *12*, 2441–2445. [CrossRef]
26. Piazza, Z.A.; Hu, H.S.; Li, W.L.; Zhao, Y.F.; Li, J.; Wang, L.S. Planar hexagonal B_{36} as a potential basis for extended single-atom layer boron sheets. *Nat. Commun.* **2014**, *5*, 3113. [CrossRef]
27. Romanescu, C.; Galeev, T.R.; Li, W.L.; Boldyrev, A.I.; Wang, L.S. Transition-metal-centered monocyclic boron wheel clusters ($M©B_n$): A new class of aromatic borometallic compounds. *Acc. Chem. Res.* **2013**, *46*, 350–358. [CrossRef]
28. Zhai, H.J.; Alexandrova, A.N.; Birch, K.A.; Boldyrev, A.I.; Wang, L.S. Hepta- and octacoordinated boron in molecular wheels of eight- and nine-atom boron clusters: Observation and confirmation. *Angew. Chem. Int. Ed.* **2003**, *42*, 6004–6008. [CrossRef]
29. Kumar, S.; Singh, M.; Sharma, D.K.; Auluck, S. Enhancing gas adsorption properties of borophene by embedding transition metals. *Comput. Condens. Matter* **2020**, *22*, e00436. [CrossRef]
30. Zhang, P.; Xu, X.; Song, E.; Hou, X.; Yang, X.; Mi, J.; Huang, J.; Stampfl, C. Transition metal-doped α-borophene as potential oxygen and hydrogen evolution electrocatalyst: A density functional theory study. *Catal. Commun.* **2020**, *144*, 106090. [CrossRef]
31. Xu, X.; Hou, X.; Lu, J.; Zhang, P.; Xiao, B.; Mi, J. Metal-doped two-dimensional borophene nanosheets for the carbon dioxide electrochemical reduction reaction. *J. Phys. Chem. C* **2020**, *124*, 24156–24163. [CrossRef]
32. Li, W.L.; Romanescu, C.; Galeev, T.R.; Piazza, Z.A.; Boldyrev, A.I.; Wang, L.S. Transition-metal-centered nine membered boron rings: $M©B_9$ and $M©B_9^-$ (M = Rh, Ir). *J. Am. Chem. Soc.* **2012**, *134*, 165–168. [CrossRef] [PubMed]
33. Zhang, J.-J.; Altalhi, T.; Yang, J.-H.; Yakobson, B.I. Semiconducting α-boron sheet with high mobility and low all-boron contact resistance: A first-principles study. *Nanoscale* **2021**, *13*, 8474–8480. [CrossRef] [PubMed]
34. Zhang, Y.-L.; Yang, J.-H.; Xiang, H.; Gong, X.-G. Fully boron sheet-based field effect transistors from first-principles: Inverse design of semiconducting boron sheets. *J. Phys. Chem. Lett.* **2021**, *12*, 576–584. [CrossRef]
35. Jiang, H.R.; Lu, Z.; Wu, M.C.; Ciucci, F.; Zhao, T.S. Borophene: A promising anode material offering high specific capacity and high rate capability for lithium-ion batteries. *Nano Energy* **2016**, *23*, 97–104. [CrossRef]
36. Jena, N.K.; Araujo, R.B.; Shukla, V.; Ahuja, R. Borophane as a bencmate of graphene: A potential 2D material for anode of Li and Na-ion batteries. *ACS Appl. Mater. Interfaces* **2017**, *9*, 16148–16158. [CrossRef]
37. Huang, C.S.; Murat, A.; Babar, V.; Montes, E.; Schwingenschlögl, U. Adsorption of the gas molecules NH_3, NO, NO_2, and CO on borophene. *J. Phys. Chem. C* **2018**, *122*, 14665–14670. [CrossRef]
38. Ta, L.T.; Hamada, I.; Morikawa, Y.; Dinh, V.A. Adsorption of toxic gases on borophene: Surface deformation links to chemisorptions. *RSC Adv.* **2021**, *11*, 18279. [CrossRef]
39. Zhao, A.; Han, Y.; Che, Y.; Liu, Q.; Wang, X.; Li, Q.; Sun, J.; Lei, Z.; He, X.; Liu, Z.H. High-quality borophene quantum dot realization and their application in a photovoltaic device. *J. Mater. Chem. A* **2021**, *9*, 24036–24043. [CrossRef]
40. Gogoi, D.; Hazarika, C.; Neog, G.; Mridha, P.; Bora, H.K.; Das, M.R.; Szunerits, S.; Boukherroub, R. Borophene quantum dots as novel peroxidase-mimicking nanozyme: A dual-mode assay for the detection of oxytetracycline and tetracycline antibiotics. *ACS Appl. Mater. Interfaces* **2024**, *16*, 14645–14660. [CrossRef]
41. Joshi, D.J.; Malek, N.I.; Jung Park, T.; Kailasa, S.K. Ultrasonication-assisted synthesis of fluorescent borophene quantum dots for sensing of dehydroepiandrosterone biomarker. *J. Mol. Liq.* **2023**, *385*, 122294. [CrossRef]
42. Yashwanth, H.J.; Hareesh, K.; Rondiya, S.R.; Choudhary, R.J.; Dhole, S.D. The borophene quantum dots scaffolded TiO_2 nanocomposite as an efficient photo electrocatalyst for water splitting application. *Appl. Surf. Sci.* **2024**, *646*, 158910. [CrossRef]
43. Ranjan, P.; Lee, J.M.; Kumar, P.; Vinu, A. Borophene: New sensation in flatland. *Adv. Mater.* **2020**, *1*, 2000531. [CrossRef] [PubMed]
44. Yadav, S.; Sadique, M.A.; Kaushik, A.; Ranjan, P.; Khan, R.; Srivastava, K.A. Borophene as an emerging 2D flatland for biomedical applications: Current challenges and future prospects. *J. Mater. Chem. B* **2022**, *10*, 1146–1175. [CrossRef]
45. Liu, X.; Hou, C.; Liu, Y.; Chen, S.; Wu, Z.; Liang, X.; Tai, G. Borophene and BC_2N quantum dot heterostructures: Ultrasensitive humidity sensing and multifunctional applications. *J. Mater. Chem. A* **2023**, *11*, 24789–24799. [CrossRef]
46. Wang, H.; An, D.; Wang, M.; Sun, L.; Li, Y.; Li, H.; Li, N.; Hu, S.; He, Y.B. Crystalline borophene quantum dots and their derivative boron nanospheres. *Mater. Adv.* **2021**, *2*, 3269–3273. [CrossRef]
47. Liang, R.; Swanson, J.M.J.; Voth, G.A. Benchmark study of the SCC-DFTB approach for a biomolecular proton channel. *J. Chem. Theory Comput.* **2014**, *10*, 451–462. [CrossRef]
48. Porezag, D.; Frauenheim, T.; Kohler, T.; Seifert, G.; Kaschner, R. Construction of tight-binding-like potentials on the basis of density-functional theory: Application to carbon. *Phys. Rev. B* **1995**, *51*, 12947. [CrossRef]
49. Elstner, M.; Porezag, D.; Jungnickel, G.; Elsner, J.; Haugk, M.; Frauenheim, T.; Suhai, S.; Seifert, G. Self-consistent-charge density-functional tight-binding method for simulation of complex materials properties. *Phys. Rev. B* **1998**, *58*, 7260. [CrossRef]
50. Frauenheim, T.; Seifert, G.; Elstner, M.; Niehaus, T.; Köhler, C.; Amkreutz, M.; Sternberg, M.; Hajnal, Z.; Di Carlo, A.; Suhai, S. Atomistic simulations of complex materials: Ground-state and excited-state properties. *J. Phys. Condens. Matter* **2002**, *14*, 3015. [CrossRef]
51. Timsorn, K.; Wongchoosuk, C. Adsorption of NO_2, HCN, HCHO and CO on pristine and amine functionalized boron nitride nanotubes by self-consistent charge density functional tight-binding method. *Mater. Res. Express* **2020**, *7*, 055005. [CrossRef]

52. Stock, B.G.; Bezugly, V.; Kunstmann, J.; Cuniberti, G.; Frauenheim, T.; Niehaus, T.A. SCC-DFTB parametrization for boron and boranes. *J. Chem. Theory Comput.* **2012**, *8*, 1153–1163. [CrossRef] [PubMed]
53. Gahrouei, M.M.; Vlastos, N.; D'Souza, R.; Odogwu, E.C.; Oliveira, L.D.S. Benchmark investigation of SCC-DFTB against standard and hybrid DFT to model electronic properties in two-dimensional MOFs for thermoelectric applications. *J. Chem. Theory Comput.* **2024**, *20*, 3976–3992. [CrossRef] [PubMed]
54. Timsorn, K.; Wongchoosuk, C. Inkjet printing of room-temperature gas sensors for identification of formalin contamination in squids. *J. Mater. Sci. Mater. Electron.* **2019**, *30*, 4782–4791. [CrossRef]
55. Marutaphan, A.; Seekaew, Y.; Wongchoosuk, C. Self-consistent charge density functional tight-binding study of poly(3,4-ethylenedioxythiphene): Poly(styrenesulfonate) ammonia gas sensor. *Nanoscale Res. Lett.* **2017**, *12*, 90. [CrossRef]
56. Arunragsa, S.; Seekaew, Y.; Pon-on, W.; Wongchoosuk, C. Hydroxyl edge-functionalized graphene quantum dots for gas-sensing applications. *Diamond Relat. Mater.* **2020**, *105*, 107790. [CrossRef]
57. Novotný, M.; Domínguez-Gutiérrez, F.J.; Krstić, P. A computational study of hydrogen detection by borophene. *J. Mater. Chem. C* **2017**, *5*, 5426–5433. [CrossRef]
58. Lukose, B.; Kuc, A.; Frenzel, J.; Heine, T. On the reticular construction concept of covalent organic frameworks. *Beilstein J. Nanotechnol.* **2010**, *1*, 60–70. [CrossRef]
59. Gemming, S.; Enyashin, A.; Andrey, N.; Frenzel, J.; Seifert, G. Adsorption of nucleotides on the rutile (110) surface. *Int. J. Mater. Res.* **2010**, *101*, 758–764. [CrossRef]
60. Wang, R.; Zhu, R.; Zhang, D. Adsorption of formaldehyde molecule on the pristine and silicon-doped boron nitride nanotubes. *Chem. Phys. Lett.* **2008**, *467*, 131–135. [CrossRef]
61. Zhai, H.J.; Kiran, B.; Li, J.; Wang, L.S. Hydrocarbon analogues of boron clusters-planarity aromaticity and antiaromaticity. *Nat. Mater.* **2003**, *2*, 827–833. [CrossRef] [PubMed]
62. Alexandrova, A.N.; Boldyrev, A.I.; Zhai, H.J.; Wang, L.S. All-boron aromatic clusters as potential new inorganic ligands and building blocks in chemistry. *Coord. Chem. Rev.* **2006**, *250*, 2811–2866. [CrossRef]
63. Qin, X.; Yan, W.; Li, D.; Zhang, Z.; Chen, S. A first-principles study of gas molecule adsorption on carbon-, nitrogen-, and oxygen-doped two-dimensional borophene. *Adv. Cond. Matter Phys.* **2021**, *2021*, 3760631. [CrossRef]
64. Zhang, C.; Zhang, Z.; Yan, W.; Qin, X. Effect of doping on the photoelectric properties of borophene. *Adv. Cond. Matter Phys.* **2021**, *3718040*, 7. [CrossRef]
65. Zhang, C.; Zhang, Z. Effect of Co-doping on the photoelectric properties of the novel two-dimensional material borophene. *Int. J. Opt.* **2023**, *1603014*, 9. [CrossRef]
66. Kistanov, A.A.; Cai, Y.; Zhou, K.; Srikanth, N.; Dmitriev, S.V.; Zhang, Y.W. Exploring the charge localization and band gap opening of borophene: A first-principles study. *Nanoscale* **2018**, *10*, 1403. [CrossRef]